Supporting Information for:

Ambient Temperature Anion-Dependent Spin State Switching Observed in "Mostly Low Spin" Heteroleptic Iron(II) Diimine Complexes

Zhaoping Ni, Ashley M. McDaniel, Matthew P. Shores*

Department of Chemistry, Colorado State University, Fort Collins, CO 80523-1872

Table of Contents

Experimental Section

Methods and Materials. All sample preparations and manipulations were performed inside a dinitrogen-filled glovebox (MBRAUN Labmaster 130). Solid state magnetic susceptibility measurements were performed with a Quantum Design model MPMS-XL superconducting quantum interference device (SQUID) magnetometer at a measuring field of 1000 G. The data were corrected for the magnetization of the sample holder by subtracting the measured susceptibility of an empty sample holder. Diamagnetic corrections were applied by using Pascal's constants.[1] ^{1}H NMR spectra were recorded using a Varian INOVA instrument operating at 400 MHz. Magnetic susceptibilities in CD_2Cl_2 solution were determined by the Evans method using TMS as the reference. Corrections for the temperature dependence of solvent density were carried out according to the data provided for CH_2Cl_2.[2-3]

Reported values include the diamagnetic corrections for the iron complexes[1] but not the solvent.[4] UV-visible spectra were recorded on a Hewlett-Packard 8453 spectrophotometer in an air-free glass cell. Infrared spectra were measured with a Nicolet 380 FT-IR using KBr pellets. Elemental analyses were performed by Robertson Microlit Laboratories Inc. in Madison, NJ. Crystallographic data were collected with a Bruker Kappa Apex 2 CCD diffractometer using graphite monochromatized $Mo_{K\alpha}$ radiation (λ = 0.71073 Å). Crystals to be analyzed at room temperature were glued to glass fibers with epoxy; those studied at 100 K were frozen to Teflon cryoloops with Paratone oil. All crystals were analyzed under a dinitrogen stream. Structures were solved by direct methods and refined with the SHELXTL software package.[5]

All solvents were sparged with dinitrogen, passed over alumina, and subjected to 3 freeze-pump-thaw cycles. The ligands 2,2′-bi-1,4,5,6-tetrahydropyrimidine (H_2bip)[6] and 2-pyridinalisopropylimine (pipi)[7] were synthesized according to the literature. All other compounds and reagents were obtained commercially and used as received.

[(H_2bip)$_2$FeBr$_2$] (1). A solution of $FeBr_2$ (1.46 g, 6.62 mmol) in 230 mL of tetrahydrofuran was combined with a solution of H_2bip (2.20 g, 13.24 mmol) in 100 mL of tetrahydrofuran, resulting in a violet suspension, then, gradually turning into orange precipitate. The mixture was stirred for 24 hours. The orange solid was collected by filtration, and washed with 30 mL of tetrahydrofuran and 20 mL of diethyl ether. Diffusion of diethyl ether into a methanolic solution of the compound afforded 2.7 g (74%) of red-orange crystals, many of which were suitable for single crystal X-ray analysis. IR (KBr): $\nu_{N\text{-}H}$ 3269, 3138 cm^{-1}; ^{1}H NMR (CD_2Cl_2): δ = 84.3, 64.7, 46.6, 40.9, 15.9, 13.4 ppm; $\chi_M T$ (300 K): 3.79 cm^3 K mol^{-1}, (5 K): 2.67 cm^3 K mol^{-1}; Elemental analysis (%) calcd for $C_{16}H_{28}N_8Br_2Fe$: C 35.06, H 5.15, N 20.44; found: C 35.10, H 5.14, N 20.27.

General procedure for synthesizing [(H_2bip)$_2$Fe(NN)]Br$_2$. To a solution of **1** (ca. 400 mg, 0.73 mmol, 1 eq) in 15 mL of methanol was added a solution of the (NN) ligand (1 eq) in 6 mL of methanol, resulting in immediate colour changes. The solution was stirred for an additional 15–45 min at room temperature, whereupon the solvent was removed in vacuo. The product was extracted into dichloromethane. The resulting mixture was filtered, and the filtrate was evaporated to obtain the [(H_2bip)$_2$Fe(NN)]Br$_2$ complex salt as a free-flowing powder. This solid was washed with ca. 15 mL of diethyl ether and dried under vacuum at room temperature for 6 h to remove trace amounts of solvent.

General procedure for synthesizing [(H_2bip)$_2$Fe(NN)](BPh$_4$)$_2$ (except for **4·BPh$_4$**, see below). A solution of [(H_2bip)$_2$Fe(NN)]Br$_2$ (approximately 0.36 mmol, 1 eq) in 11 mL of methanol was gradually added to a solution of excess $NaBPh_4$ (4 eq) in 10 mL of methanol, resulting in the formation of a coloured precipitate. The mixture was stirred for an additional 15–30 min at room temperature. The solid was collected by filtration, washed with methanol (10 mL) and diethyl ether (10 mL), and dried to obtain [(H_2bip)$_2$Fe(NN)](BPh$_4$)$_2$ as a powdered product.

Note on ^{1}H NMR characterization. The spectra of [(H_2bip)$_2$Fe(NN)](BPh$_4$)$_2$ complexes show some ligand dissociation even in CD_2Cl_2. Resonances for [Fe(H_2bip)$_3$]$^{2+}$ are not included in the listings below, but are clearly marked in Figures S6 and S9-10. These signals emerge after the salts have been left in solution overnight. The

CH_2 proton environments on the H_2bip ligand are magnetically non-equivalent and produce a complicated resonance pattern in the range of 1.5~4.5 ppm for the bromide salts. In addition, the tetraphenylborate salts show significant shifts in these resonances. Generally, these protons were not assigned in the following listings (except **3**–**4·Br**) or in the figures of ^{1}H NMR spectra.

[(H$_2$bip)$_2$Fe(pipi)]Br$_2$ (2·Br). 115 mg of 2-pyridinalisopropylimine (pipi, 0.78 mmol) was combined with 425 mg of **1**, affording 523 mg of product (97 %). IR (KBr): $\nu_{N\text{-}H}$ 3223, 3123 cm^{-1}; ^{1}H NMR (CD_2Cl_2): δ = 13.2 (CH), 11.2 (NH), 11.0 (CH & NH), 10.7 (NH), 10.5 (NH), 8.5 (aryl), 8.1 (aryl), 6.5 (CH), 4.2, 4.0, 3.9, 3.8, 3.3, 3.2, 2.9, 2.8, 2.6, 2.3, 2.2, 2.0, 1.9, 1.8 (CH_3), 1.4 ppm (CH_3); UV/Vis (CH_2Cl_2): λ_{max} (ε [M^{-1} cm^{-1}]) = 457 (6760), 699 nm (5760); $\chi_M T$ (300 K): 0.56 cm^3 K mol^{-1}; *m*/*z* 552 (5%) [Fe(H$_2$bip)$_2$(H$_2$bip–H)]$^+$, 467 (100) [Fe(H$_2$bip)$_2$Br]$^+$, 449 (9) [Fe(H$_2$bip)(pipi)Br]$^+$, 387 (69) [Fe(H$_2$bip)(H$_2$bip–H)]$^+$, 369 (13) [Fe(H$_2$bip–H)(pipi)]$^+$, 301 (61) [Fe(H$_2$bip)Br]$^+$, 167 (64) [H$_2$bip+H]$^+$; Elemental analysis (%) calcd for $C_{25}H_{40}N_{10}Br_2Fe$: C 43.12, H 5.79, N 20.12; found: C 42.85, H 5.81, N 19.89.

[(H$_2$bip)$_2$Fe(pipi)](BPh$_4$)$_2$ (2·BPh$_4$). 220 mg of **2·Br** (0.32 mmol) was combined with 433 mg of $NaBPh_4$, affording 356 mg of product (96 %). IR (KBr): $\nu_{N\text{-}H}$ 3385 cm^{-1}; ^{1}H NMR (CD_2Cl_2): δ = 37.6 (CH), 32.7 (aryl), 25.0 (aryl), 17.4 (NH), 15.8 (aryl), 15.1 (NH), 14.5 (NH) , 12.1 (aryl), 10.2 (aryl), 9.5, 9.1, 7.8 (BPh_4), 7.3 (BPh_4), 7.1 (BPh_4), 6.8, 6.0, 5.7, 5.5, 5.3, 5.0, 4.6, 4.1, 3.9, 3.3, 2.1, 1.9, –0.8, –2.6 ppm; UV/Vis (CH_2Cl_2): λ_{max} (ε [M^{-1} cm^{-1}]) = 448 (5220), 674 nm (4880); $\chi_M T$ (300 K): 0.32 cm^3 K mol^{-1}; *m*/*z* 387 (100%) [Fe(H$_2$bip)(H$_2$bip–H)]$^+$, 369 (14) [Fe(H$_2$bip–H)(pipi)]$^+$, 167 (7) [H$_2$bip+H]$^+$; Elemental analysis (%) calcd for $C_{73}H_{80}N_{10}B_2Fe$: C 74.62, H 6.86, N 11.92; found: C 74.45, H 7.05, N, 11.79. Crystals of **2·BPh$_4$** suitable for X-ray analysis were grown by slow diffusion of diethyl ether into a concentrated acetonitrile solution of **2·BPh$_4$**.

[(H$_2$bip)$_2$Fe(bpy)]Br$_2$ (3·Br). 115 mg of 2,2′-bipyridine (bpy, 0.74 mmol) was combined with 400 mg of **1**, affording 482 mg of product (93 %). IR (KBr): $\nu_{N\text{-}H}$ 3221, 3122 cm^{-1}; ^{1}H NMR (CD_2Cl_2): δ = 9.9 (d, 4H, NH), 9.1 (d, 2H, aryl), 8.5 (d, 2H, aryl), 7.9 (t, 2H, aryl), 7.8 (t, 2H, aryl), 3.9 (br, 2H, CH), 3.8 (br, 2H, CH), 3.6 (br, 2H, CH), 3.5 (br, 2H, CH), 2.8 (br, 4H, CH), 2.5 (br, 2H, CH), 2.2 (br, 2H, CH), 2.1 (br, 2H, CH), 1.9 (br, 2H, CH), 1.7 (br, 4H, CH) ppm; UV/Vis (CH_2Cl_2): λ_{max} (ε [M^{-1} cm^{-1}]) = 443 (9530), 687 nm (4620); $\chi_M T$ (300 K): 0.20 cm^3 K mol^{-1}; *m*/*z* 552 (4%) [Fe(H$_2$bip)$_2$(H$_2$bip–H)]$^+$, 467 (100) [Fe(H$_2$bip)$_2$Br]$^+$, 457 (26) [Fe(H$_2$bip)(bpy)Br]$^+$, 387 (45) [Fe(H$_2$bip)(H$_2$bip–H)]$^+$, 301 (71) [Fe(H$_2$bip)Br]$^+$, 167 (34) [H$_2$bip+H]$^+$; Elemental analysis (%) calcd for $C_{26}H_{36}N_{10}Br_2Fe$: C 44.34, H 5.15, N 19.89; found: C 44.09, H 4.91, N 19.61.

[(H$_2$bip)$_2$Fe(bpy)](BPh$_4$)$_2$ (3·BPh$_4$). 262 mg of **3·Br** (0.37 mmol) was combined with 509 mg of $NaBPh_4$, affording 404 mg of product (92 %). IR (KBr): $\nu_{N\text{-}H}$ 3381, 3297 cm^{-1}; ^{1}H NMR (CD_2Cl_2): δ = 14.8 (aryl), 10.2 (aryl), 9.4 (aryl), 8.9 (NH), 8.3 (aryl), 8.1 (NH), 7.7 (BPh_4), 7.2 (BPh_4), 7.1 (BPh_4), 5.3, 4.6, 4.2, 4.0, 2.7, 2.4, 1.7, 1.2 ppm; UV/Vis (CH_2Cl_2): λ_{max} (ε [M^{-1} cm^{-1}]) = 438 (6920), 482 (sh, 6500), 601 (3810), 656 nm (3940); $\chi_M T$ (300 K): 0.16 cm^3 K mol^{-1}; *m*/*z* 387 (100%) [Fe(H$_2$bip)(H$_2$bip–H)]$^+$, 377 (20) [Fe(H$_2$bip–H)(bpy)]$^+$, 167 (14)

$[H_2bip+H]^+$; Elemental analysis (%) calcd for $C_{74}H_{76}N_{10}B_2Fe$: C 75.14, H 6.48, N 11.84; found: C 74.95, H 6.74, N 11.74. Crystals of **3·BPh$_4$**·~1.2MeCN suitable for X-ray analysis were grown by slow diffusion of diethyl ether into a concentrated acetonitrile solution of **3·BPh$_4$**.

[(H$_2$bip)$_2$Fe(phen)]Br$_2$ (4·Br). 137 mg of 1,10-phenanthroline (phen, 0.75 mmol) was combined with 413 mg of **1**, affording 438 mg of product (81 %). IR (KBr): $\nu_{N\text{-}H}$ 3219, 3127 cm^{-1}; ^{1}H NMR (CD_2Cl_2): δ = 10.6 (s, 2H, aryl), 10.5 (d, 4H, NH), 8.5 (d, 2H, aryl), 8.4 (d, 2H, aryl), 8.2 (s, 2H, aryl), 4.1 (br, 2H, CH), 4.0 (br, 2H, CH), 3.6 (br, 4H, CH), 2.9 (br, 2H, CH), 2.7 (br, 4H, CH), 2.2 (br, 4H, CH), 1.9 (br, 2H, CH), 1.7 (br, 4H, CH) ppm; UV/Vis (CH_2Cl_2): λ_{max} (ε [M^{-1} cm^{-1}]) = 398 (sh, 3860), 468 (5840), 607 (6360), 666 nm (6250); $\chi_M T$ (300 K): 0.15 cm^3 K mol^{-1}; *m*/*z* 552 (2%) $[Fe(H_2bip)_2(H_2bip–H)]^+$, 495 (31) $[Fe(phen)_2Br]^+$, 481 (100) $[Fe(H_2bip)(phen)Br]^+$, 467 (31) $[Fe(H_2bip)_2Br]^+$, 401 (46) $[Fe(H_2bip–H)(phen)]^+$, 387 (13) $[Fe(H_2bip)(H_2bip–H)]^+$, 315 (14) $[Fe(phen)Br]^+$, 301 (21) $[Fe(H_2bip)Br]^+$, 181 (3) $[phen+H]^+$, 167 (8) $[H_2bip+H]^+$; Elemental analysis (%) calcd for $C_{28}H_{36}N_{10}Br_2Fe$: C 46.18, H 4.98, N 19.23; found: C 45.89, H 4.89, N 18.98.

[(H$_2$bip)$_2$Fe(phen)](BPh$_4$)$_2$·0.4CH$_2$Cl$_2$ (4·BPh$_4$·0.4CH$_2$Cl$_2$). Similar to the general procedure, 212 mg of **4·Br** (0.37 mmol) was combined with 398 mg of $NaBPh_4$, affording 304 mg of crude product. The product was extracted into dichloromethane. The mixture was filtered, and the filtrate was precipitated in 20 mL diethyl ether. The solid was collected by filtration, washed with methanol (10 mL) and diethyl ether (10 mL), and dried to obtain 220 mg product (61%). IR (KBr): $\nu_{N\text{-}H}$ 3380 cm^{-1}; ^{1}H NMR (CD_2Cl_2): δ = 20.7 (aryl), 12.1 (NH), 11.0 (aryl & NH), 9.2 (aryl), 8.7 (aryl), 7.7 (BPh_4), 7.2 (BPh_4), 7.1 (BPh_4), 5.6, 5.4, 4.9, 4.4, 3.4, 3.2, 2.9, 1.6 ppm; UV/Vis (CH_2Cl_2): λ_{max} (ε [M^{-1} cm^{-1}]) = 395 (sh, 2730), 485 (5810), 581 (6010), 647 nm (sh, 4910); $\chi_M T$ (300 K): 0.50 cm^3 K mol^{-1}; *m*/*z* 581 (2%) $[Fe(H_2bip–H)(phen)_2]^+$, 401 (100) $[Fe(H_2bip–H)(phen)]^+$, 387 (26) $[Fe(H_2bip)(H_2bip–H)]^+$, 181 (3) $[phen+H]^+$, 167 (6) $[H_2bip+H]^+$; Elemental analysis (%) calcd for $C_{76}H_{76}N_{10}B_2Fe·0.4CH_2Cl_2$: C 73.95, H 6.24, N 11.29; found: C 73.82, H 6.23, N 11.58. The inclusion of 0.4 equivalents of dichloromethane solvate in powdered samples was reproducible, and confirmed by identification in ^{1}H NMR spectra collected in CD_3CN. Since the salt was studied in dichloromethane solutions, it was not dried at higher temperatures to remove the solvent. Crystals of **4·BPh$_4$**·~2.55CH_2Cl_2 were grown by diffusion of diethyl ether into a dichloromethane solution of **4·BPh$_4$**.

X-Ray Structure Determinations. The crystallographic data, selected bond distances and Σ[8-9] and Θ[10] distortion parameters are presented in Table S1. Unless otherwise noted, thermal parameters for all fully occupied, non-hydrogen atoms were refined anisotropically. Hydrogen atoms were added at the ideal positions and were refined using a riding model where the thermal parameters were set at 1.2 times those of the attached carbon atom (1.5 times that for methyl protons). The crystal used for compound **1** is monoclinic with β ~ 90°, and showed signs of pseudomerohedral twinning. Both components of the twinned crystal are related by a two-fold rotation around the *a* axis, requiring the use of the twin law 1 0 0 0 –1 0 0 0 –1 to produce a successful refinement. The

two components refined to an 80:20 ratio. The ancillary bpy ligand in the structure of **3·BPh$_4$** is crystallographically disordered with respect to one of the H_2bip ligands; nevertheless the disordered components refine to the expected 2:1 H_2bip:bpy ratio. After significant attempts to model severe solvent disorder in the structures of **3·BPh$_4$** (~1.2 CH_3CN) and **4·BPh$_4$** (~2.55 CH_2Cl_2) failed to produce satisfactory results, SQUEEZE[11] was used to remove the disordered species. Further refinement details, including treatment of compositional and/or site occupancy disorder, are presented in cif format. CCDC 768562 (**1**), 768563 (**2·BPh$_4$**), 768564 (**3·BPh$_4$**) and 768565 (**4·BPh$_4$**) contain the supplementary crystallographic data for this paper. These data can be obtained free of charge from the Cambridge Crystallographic Data Centre via www.ccdc.cam.ac.uk/data_request/cif.

Thermodyamics parameters: The temperature dependence of solution magnetic susceptibility data for **2·BPh$_4$**–**4·BPh$_4$** were fit to HS-LS equlibrium expressions modified from the literature:[12]

$$\chi T_{\text{species}} = \frac{\left[\frac{g_{\text{HS}}{}^2}{4} C_{\text{HS}} + TIP_{\text{HS}} * T\right] - \left[\frac{g_{\text{LS}}{}^2}{4} C_{\text{LS}} + TIP_{\text{LS}} * T\right]}{1 + \exp\left[\frac{\Delta H}{R} * \left(\frac{1}{T} - \frac{1}{T_c}\right)\right]} + \left[\frac{g_{\text{LS}}{}^2}{4} C_{\text{LS}} + TIP_{\text{LS}} * T\right] \quad \text{(S1)}$$

$$\chi T_{\text{exp}} = (1 - a) * \chi T_{[\text{Fe}(\text{H}_2\text{bip})_2(\text{NN})]} + a * \chi T_{[\text{Fe}(\text{H}_2\text{bip})_3]} \quad \text{(S2)}$$

where g_{HS} and g_{LS} are the Landé factors of the S = 2 and S = 0 states, respectively; C and TIP are the Curie constants and temperature-independent paramagnetism terms, respectively; R is the gas constant; ΔH is the enthalpy term; and T_c is the critical temperature (where HS:LS ratio is 50:50). The entropy term is calculated from the expression $\Delta S = \Delta H/T_c$. Equation S1 is taken from a report by Berry and coworkers;[12] here we do not fit g_{LS} since $C_{\text{LS}} = 0$ for the diamagnetic LS species. Equation S2 accounts for the presence of a second SC-active species: parameter a represents the amount of impurity $[Fe(H_2bip)_3]^{2+}$ that contributes to the observed susceptibility properties. The parameters for the $[Fe(H_2bip)_3]^{2+}$ complex[13] were fit by equation S1 with g_{HS} fixed at 2.11.[14] The parameters for the $[Fe(H_2bip)_2(NN)]^{2+}$ complexes and a value were then fit to equation S2 by using the fitted parameters of the $[Fe(H_2bip)_3]^{2+}$ complex. The g_{HS} value was set at 2.11 for all the heteroleptic complexes. Reasonable fits could be obtained only when TIP_{HS} was manually set for the $[Fe(H_2bip)_2(NN)]^{2+}$ complexes. The fitting results are summarized in Table S2.

Anion binding titration studies: *a) Via ^{1}H NMR spectroscopy*. The host solutions were prepared in CD_2Cl_2 with the concentrations of 5.1, 6.2 and 5.9 mM for **2**–**4·BPh$_4$**, respectively. Stock solutions of Bu_4NBr were prepared in CH_2Cl_2 at concentrations 10 times that of the respective host solutions. Different equivalents of guest solutions were added into air-free NMR tubes via a 100 μL syringe, and the solvent was carefully removed *in vacuo* to avoid dilution effects. Then the host solutions (0.5 mL) were added into each NMR tubes with different equivalents of dried Bu_4NBr (up to 5 equiv), and ^{1}H NMR spectra were obtained on a Varian INOVA instrument

operating at 400 MHz. The diamagnetic correction for Bu_4NBr was determined experimentally in a concentration range, [L], from 50 to 300 mM in CD_2Cl_2 at 296 K as shown in Figure S8. The linear concentration dependence was found: $\Delta\delta = -0.0906*[L]$, where $\Delta\delta$ (in ppm) is the chemical-shift difference between the resonances of TMS in the two coaxial tubes.[15] *b) Via UV-Visible spectroscopy*. Stock solutions of the host molecule were prepared in CH_2Cl_2 with the concentrations of 0.9×10^{-4}, 0.6×10^{-4} and 1.0×10^{-4} M for **2**–**4**·**BPh$_4$**, respectively. Guest solutions were prepared by the addition of 100 equivalents of solid Bu_4NBr into the respective host solutions. Typically, a 4 mL host solution was added into an air-free spectrometric cell. Small aliquots (5–40 μL) of the guest solution were added to the cell using a 100 μL syringe and the UV-Visible spectra were collected after each addition (up to 11 equiv added in total). All spectrophotometric titration curves were fitted with the 1stOpt 3.0 program.[16] The Global Levenberg-Marquardt method was used to determine the non-linear regressions. Binding constants were obtained from a simultaneous fit of the electronic absorption spectral changes at four selected wavelengths in the range 430–740 nm.. The titration sequence was repeated three times for the phen-containing complex **4**·**BPh$_4$**, and provides average log*K* values with error estimates of ±13%,

Control experiments. In recognition that ligand dissociation occurs even in CD_2Cl_2 (see *Note on ^{1}H NMR characterization* on p. S-2), additional stability checks were performed on **2**–**4**·**BPh$_4$** using pure crystalline samples. First, the measured susceptibilities of the host solutions change by no more than 0.02 cm^3 K mol^{-1} after 140 minutes, longer than the length of time required to perform titration experiments. Second, the susceptibilities of these solutions mixed with five equivalents of Bu_4NBr change by no more than 0.01 cm^3 K mol^{-1} after 140 min beyond the initial change due to anion-dependent spin state switching. Third, as shown in Figures S12–14, the changes in chemical shifts for protons on the complex cations are less than 0.2 ppm after spiking the NMR sample with 0.5 equivalents of paramagnetic $[Fe(H_2bip)_3](BPh_4)_2$. This is very small compared to the obvious upfield $\Delta\delta$ (–7.8 ppm) which can be observed for the α–H on the pipi ligand after the addition of 0.5 equivalents of Bu_4NBr. We also note that the protons on BPh_4^- anions can show downfield shifts of 0.8 ppm after the addition of 0.5 equivalents of $[Fe(H_2bip)_3](BPh_4)_2$, which suggests that the cations do interact with tetraphenylborate to some extent in dichloromethane solution. The fact that the cation resonances are largely insensitive to paramagnetic impurities means that chemical shift changes can be used to probe anion binding and spin state switching without significant signal contamination from trace impurities; *also, while ligand dissociation may reduce the number of spin-switching capable species in solution, it cannot affect the HS:LS ratio which is responsible for the observed chemical shifts of the sensing complex*. These results demonstrate that, although ligand dissociation is a potentially complicating factor, the desired $[(H_2bip)_2Fe(NN)]^{2+}$ complexes **2-4** are largely intact in dichloromethane solution, and the property changes arising from anion-binding are much more significant than those attributable to other sources.

References for Supporting Information:

1 O. Kahn, *Molecular Magnetism*, VCH: New York, 1993.
2 D. Ostfeld and I. A. Cohen, *J. Chem. Educ.*, 1972, **49**, 829.
3 C. L. Yaws, *Thermodynamic and Physical Property Data*, Gulf Publishing Co.; Houston, 1992, p 96.
4 D. H. Grant, *J. Chem. Educ.*, 1995, **72**, 39.
5 G. M. Sheldrick, *SHELXTL, Version 6.14;* Bruker Analytical X-Ray Systems, Inc.: Madison, WI, 1999.
6 M. G. Burnett, V. McKee and S. M. Nelson, *J. Chem. Soc., Dalton Trans.*, 1981, 1492-1497.
7 M. A. Robinson, J. D. Curry and D. H. Busch, *Inorg. Chem.*, 1963, **2**, 1178-1181.
8 M. G. B. Drew, C. J. Harding, V. McKee, G. G. Morgan and J. Nelson, *J. Chem. Soc., Chem. Commun.*, 1995, 1035-1038.
9 P. Guionneau, M. Marchivie, G. Bravic, J.-F. Létard and D. Chasseau, *J. Mater. Chem.*, 2002, **12**, 2546-2551.
10 M. Marchivie, P. Guionneau, J.-F. Létard and D. Chasseau, *Acta Crystallogr.*, 2005, **B61**, 25-28.
11 P. V. D. Sluis and A. L. Spek, *Acta Crystallogr.*, 1990, **A46**, 194-201.
12 J. F. Berry, F. A. Cotton, T. Lu and C. A. Murillo, *Inorg. Chem.*, 2003, **42**, 4425-4430.
13 Z. Ni and M. P. Shores, *J. Am. Chem. Soc.*, 2009, **131**, 32-33.
14 A. Ozarowski, S. A. Zvyagin, W. M. Reiff, J. Telser, L.-C. Brunel and J. Krzystek, *J. Am. Chem. Soc.*, 2004, **126**, 6574-6575.
15 W. Linert, M. Konecny and F. Renz, *J. Chem. Soc., Dalton Trans.*, 1994, 1523-1531.
16 *1stOpt 3.0;* 7D-Soft High Technology Inc., Beijing, China, 2009.

Table S1. Crystallographic data and selected structural observations for compounds $[(H_2bip)_2FeBr_2]$ (**1**), $[(H_2bip)_2Fe(pipi)](BPh_4)_2$ (**2·BPh$_4$**), $[(H_2bip)_2Fe(bpy)](BPh_4)_2$ (**3·BPh$_4$**) and $[(H_2bip)_2Fe(phen)](BPh_4)_2$ (**4·BPh$_4$**)[a].

	1	**2·BPh$_4$**	**3·BPh$_4$**	**4·BPh$_4$**
formula	$C_{16}H_{28}Br_2FeN_8$	$C_{73}H_{80}B_2FeN_{10}$	$C_{74}H_{76}B_2FeN_{10}$	$C_{76}H_{76}B_2FeN_{10}$
colour	red-orange	green	olive	indigo
habit	block	slide	block	needle
M	548.11	1174.94	1182.92	1206.94
T [K]	296	100	100	100
system	monoclinic	triclinic	triclinic	monoclinic
space group	$P2_1/n$	$P\bar{1}$	$P\bar{1}$	$C2/c$
Z	4	2	2	8
a [Å]	9.5341(6)	13.1775(3)	13.040(3)	45.6638(8)
b [Å]	16.1645(12)	13.2415(3)	13.169(3)	12.6323(2)
c [Å]	13.7170(8)	18.3584(4)	22.292(5)	24.6196(4)
α [°]	90	93.460(1)	76.65(3)	90
β [°]	90.539(4)	97.330(1)	79.24(3)	98.8310(10)
γ [°]	90	90.471(1)	60.99(3)	90
V [Å^3]	2113.9(2)	3170.98(12)	3244.7(16)	14033.2(4)
ρ_{calcd} [g/cm^3]	1.722	1.231	1.211	1.143
GOF	1.114	1.031	1.082	1.019
$R_1(wR_2)$[b], %	5.64(19.54)	6.98(19.28)	6.12(18.31)	5.63(16.53)
avg Fe–N(H_2bip) [Å]	2.132(9)	1.980(3)	1.985(5)	1.979(2)
avg Fe–N(NN) [Å]		1.950(3)	1.953(7)	1.965(2)
avg Fe–N(all) [Å][c]	2.132(9)	1.970(3)	1.972(6)	1.974(2)
Σ[°][d]	71.86(2)	63.79(12)	69.7(2)	58.46(8)
Θ[°][d]	190.9	137.6	131.3	126.4

[a] The parameters presented here reflect solvent-free data. [b] $R_1 = \Sigma||F_o| - |F_c||/\Sigma|F_o|$, $wR_2 = \{\Sigma[w(F_o^2 - F_c^2)^2]/\Sigma[w(F_o^2)^2]\}^{1/2}$ for $F_o > 4\sigma(F_o)$. [c] Average value for all Fe-N distances in the structure. [d] For determinations of Σ and Θ, see references 8-10.

Table S2. Fitted thermodynamic parameters for SC behaviour in the iron complexes **2·BPh$_4$**–**4·BPh$_4$**.

complex	TIP_{HS} ($cm^3\ mol^{-1}$)	TIP_{LS} ($cm^3\ mol^{-1}$)	ΔH^a ($kJ\ mol^{-1}$)	ΔS^a ($J\ K^{-1}\ mol^{-1}$)	T_c (K)	*a*
$[Fe(H_2bip)_3](BPh_4)_2$	0.0009(2)	0.002(2)	11(1)	55	201(9)	
2·BPh$_4$	0.0010	0.0010(1)	26(1)	71	367(2)	0.01(2)
3·BPh$_4$	0.0008	0.0008(1)	28(1)	70	402(6)	0.01(1)
4·BPh$_4$	0.0008	0.0008(2)	25(2)	65	386(6)	0.02(2)

[a] The enthalpy and entropy changes associated with the LS→HS conversion are generally on the order of ΔH = 6–25 kJ mol^{-1} and ΔS = 50–80 J K^{-1} mol^{-1}. Reference: J. England, G. J. P. Britovsek, N. Rabadia and A. J. P. White, *Inorg. Chem.*, 2007, **46**, 3752-3767 and references therein.

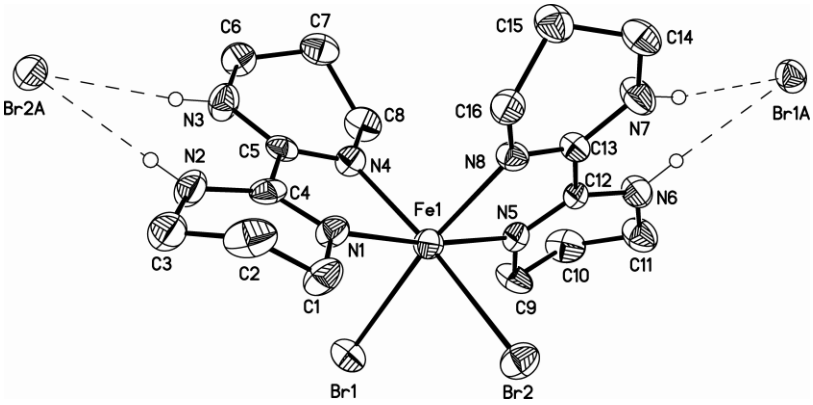

Figure S1. The asymmetric unit in the crystal structure of **1·Br** at 296 K, drawn with 40% probability ellipsoids. Hydrogen atoms bound to C atoms are removed for clarity. The complex resides on a general position. Br1A and Br2A are coordinated to neighboring complexes, and have been copied from their original positions to (x–1/2, –y+1/2, z+1/2) and (x–1/2, –y+1/2, z–1/2), respectively. The hydrogen bonding interactions are N2···Br2A = 3.400(9) Å, N3···Br2A = 3.385(10) Å, N6···Br1A = 3.351(9) Å, N7···Br1A = 3.370(10) Å.

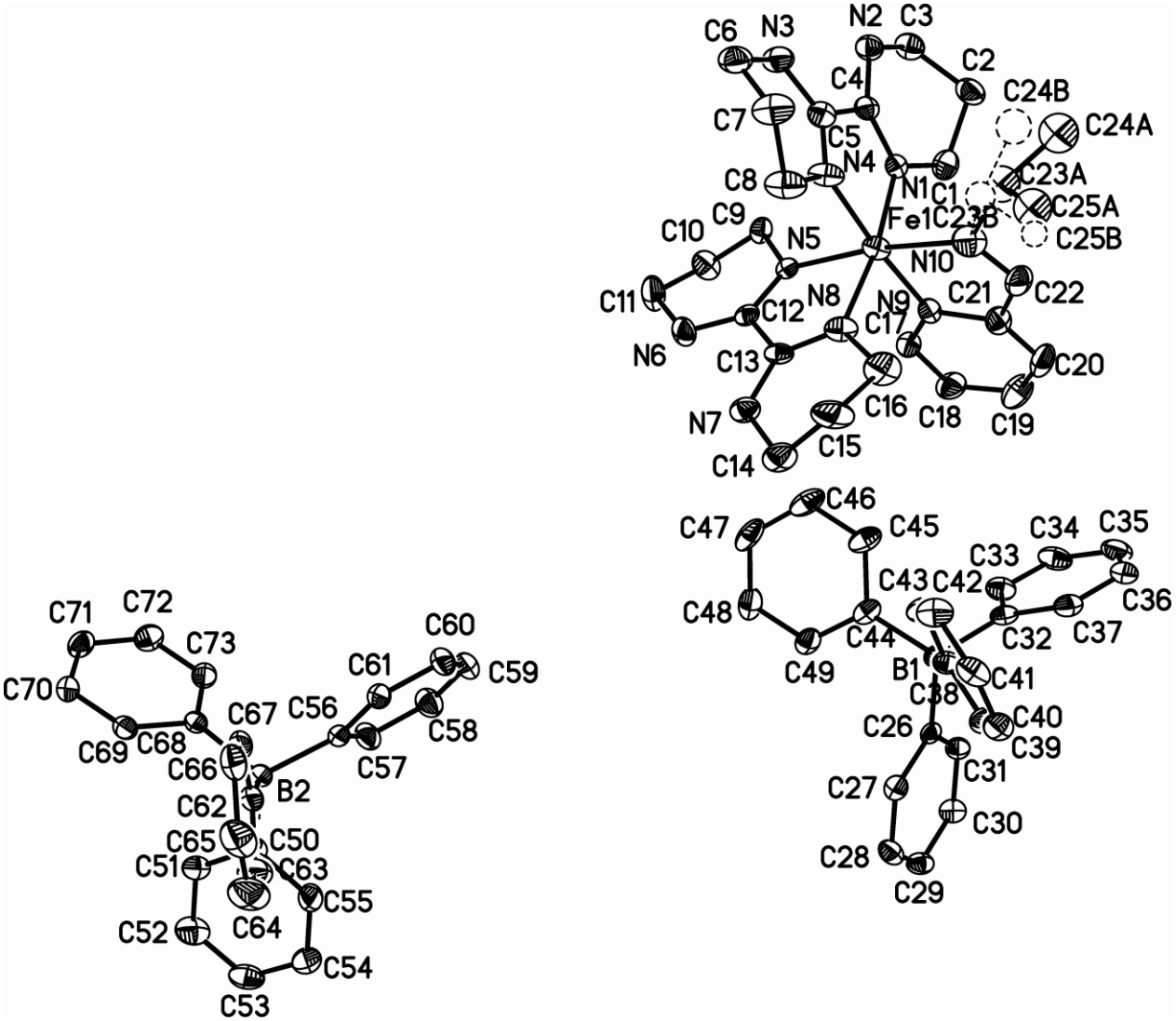

Figure S2. The asymmetric unit in the crystal structure of **2·BPh$_4$** at 100 K, drawn with 40% probability ellipsoids. All hydrogen atoms have been omitted for clarity. The disordered atoms are labeled with suffixes "A" and "B". The closest cation-anion contact is N3···C73 (–x+1, –y, –z+1) = 3.315(5) Å.

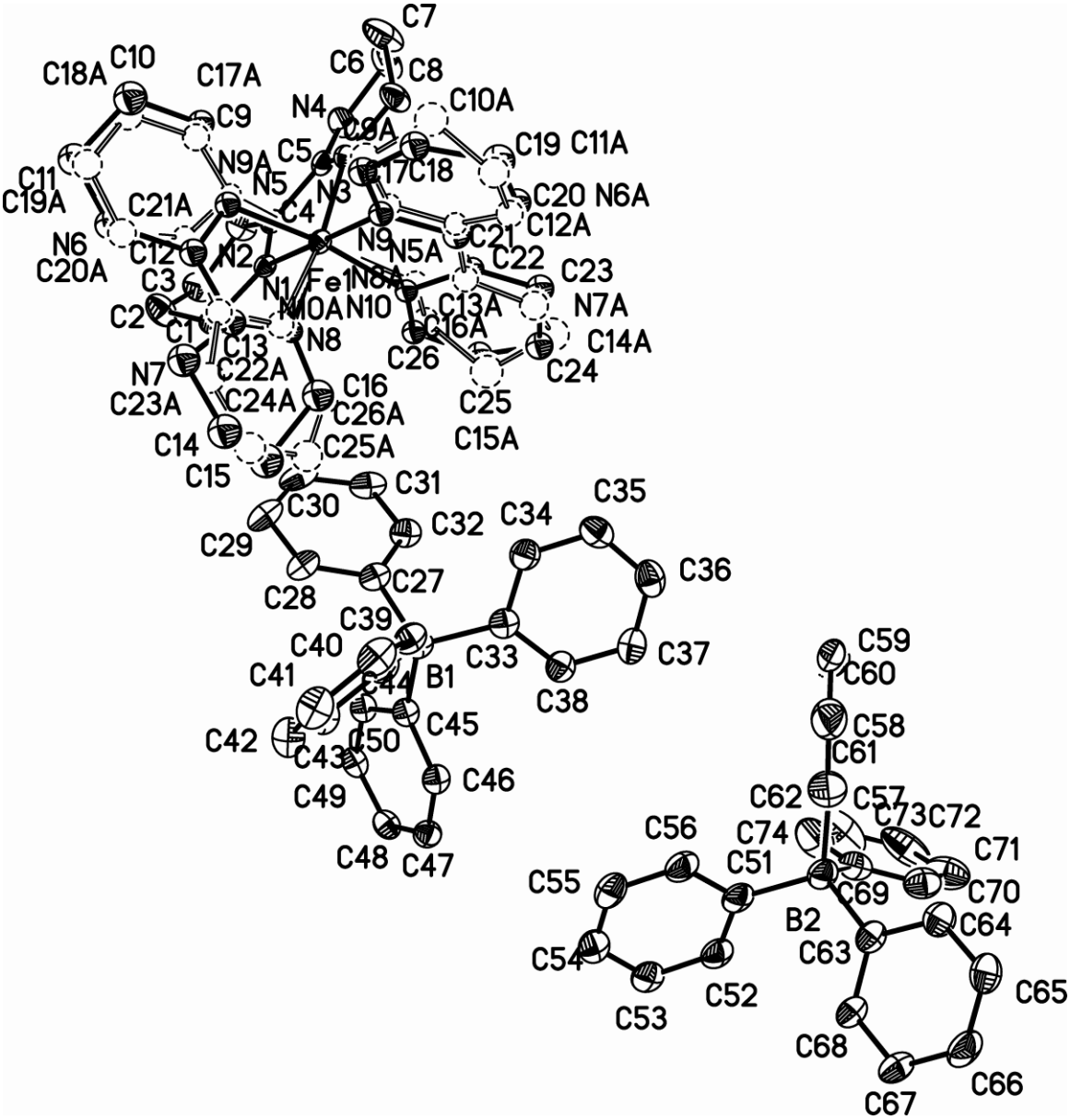

Figure S3. The asymmetric unit in the crystal structure of **3·BPh$_4$**, drawn with 40% probability ellipsoids. All hydrogen atoms have been omitted for clarity. The three ligand sites on the Fe appear to be occupied as: (a) 100% (H_2bip), (b) 50% (H_2bip)/50%(bpy), (c) 50%(bpy)/50%(H_2bip); the overall chemical formula refines to [Fe(H_2bip)$_2$bpy](BPh$_4$)$_2$.The disordered atoms are labelled with suffixes "A" and "B". The closest cation-anion contact is N3···C40 (x, y+1, z) = 3.288(3) Å.

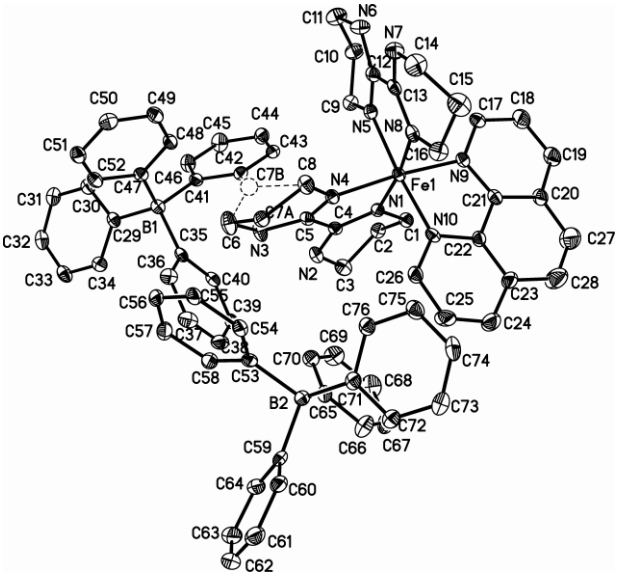

Figure S4. The asymmetric unit in the crystal structure of **4·BPh$_4$** at 100 K, drawn with 40% probability ellipsoids. All hydrogen atoms have been omitted for clarity. The disordered atoms are labelled with suffixes "A" and "B". The closest cation-anion contact is N6···C48 (–x, y, –z+1/2) = 3.197(3) Å.

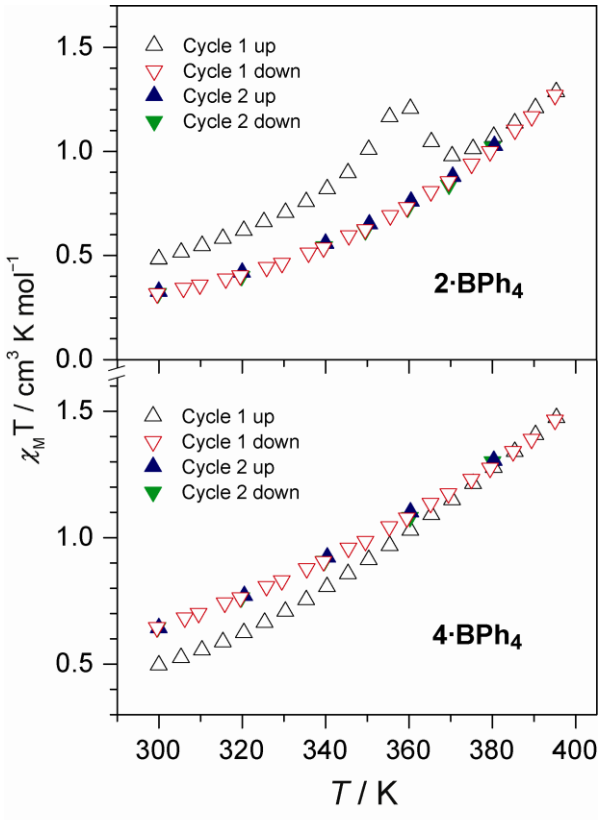

Figure S5. Temperature dependence of the magnetic susceptibilities for samples of **2·BPh$_4$** (crystal) and **4·BPh$_4$·0.4CH$_2$Cl$_2$** (powder). The pipi-containing crystals likely represent surface acetonitrile, which was removed by heating the sample. The susceptibility for the phen-containing sample is presented as if the molecular weight of the compound does not change during the course of the experiment.

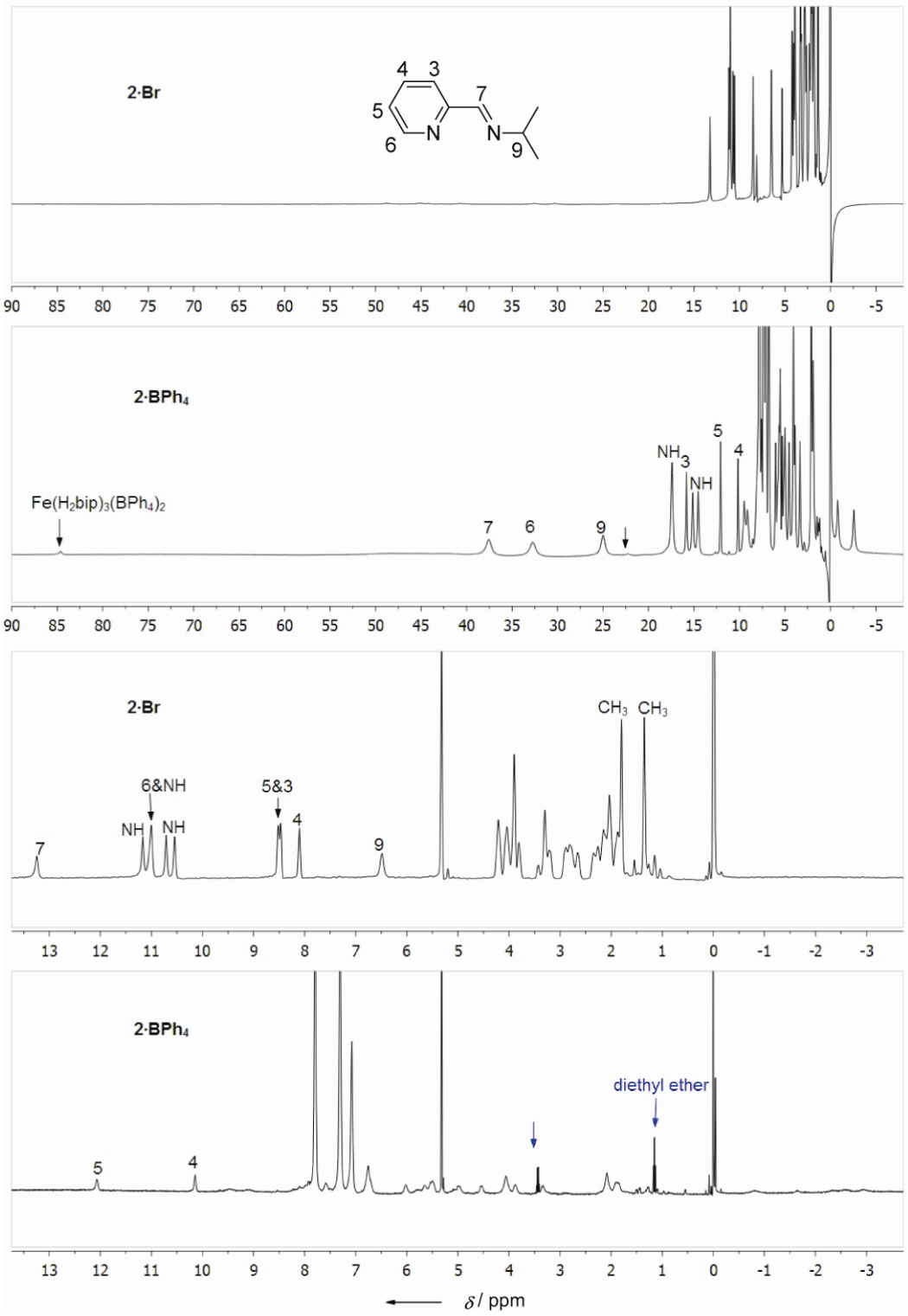

Figure S6. ^{1}H NMR spectra (expanded and normal windows) for salts of pipi-containing **2** at 296 K (400 MHz, CD_2Cl_2).

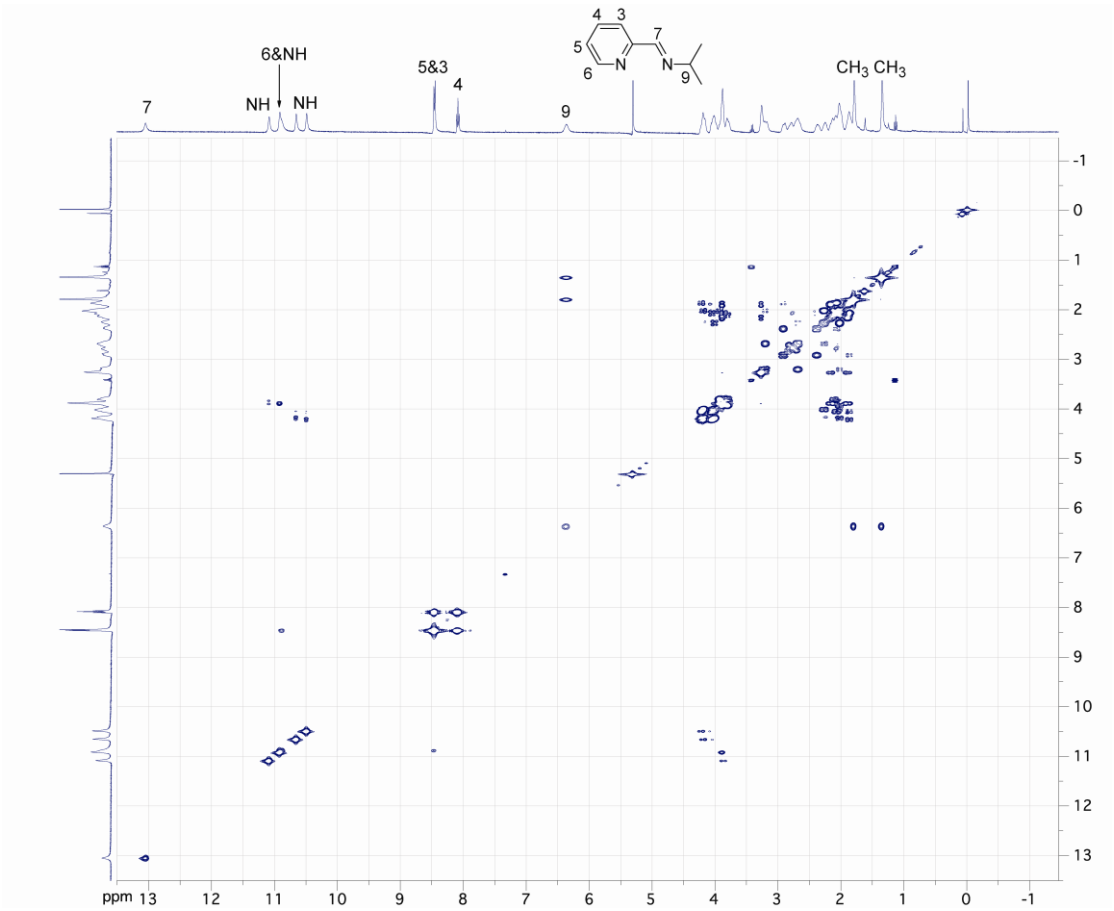

Figure S7. The ^{1}H COSY (400 MHz) NMR spectrum of **2·Br** recorded in CD_2Cl_2 at 296 K.

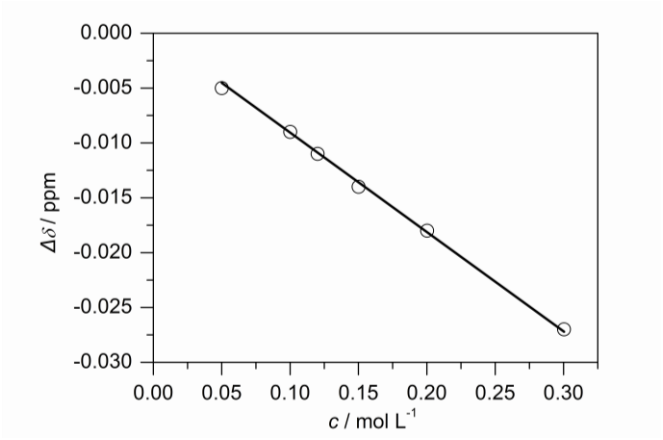

Figure S8. Concentration dependence of the diamagnetic contribution for Bu_4NBr in CD_2Cl_2 at 296 K. Below salt concentrations of 0.05 M, we cannot observe two different TMS signals. Note that titration experiments were carried out at salt concentrations no greater than 0.031 M.

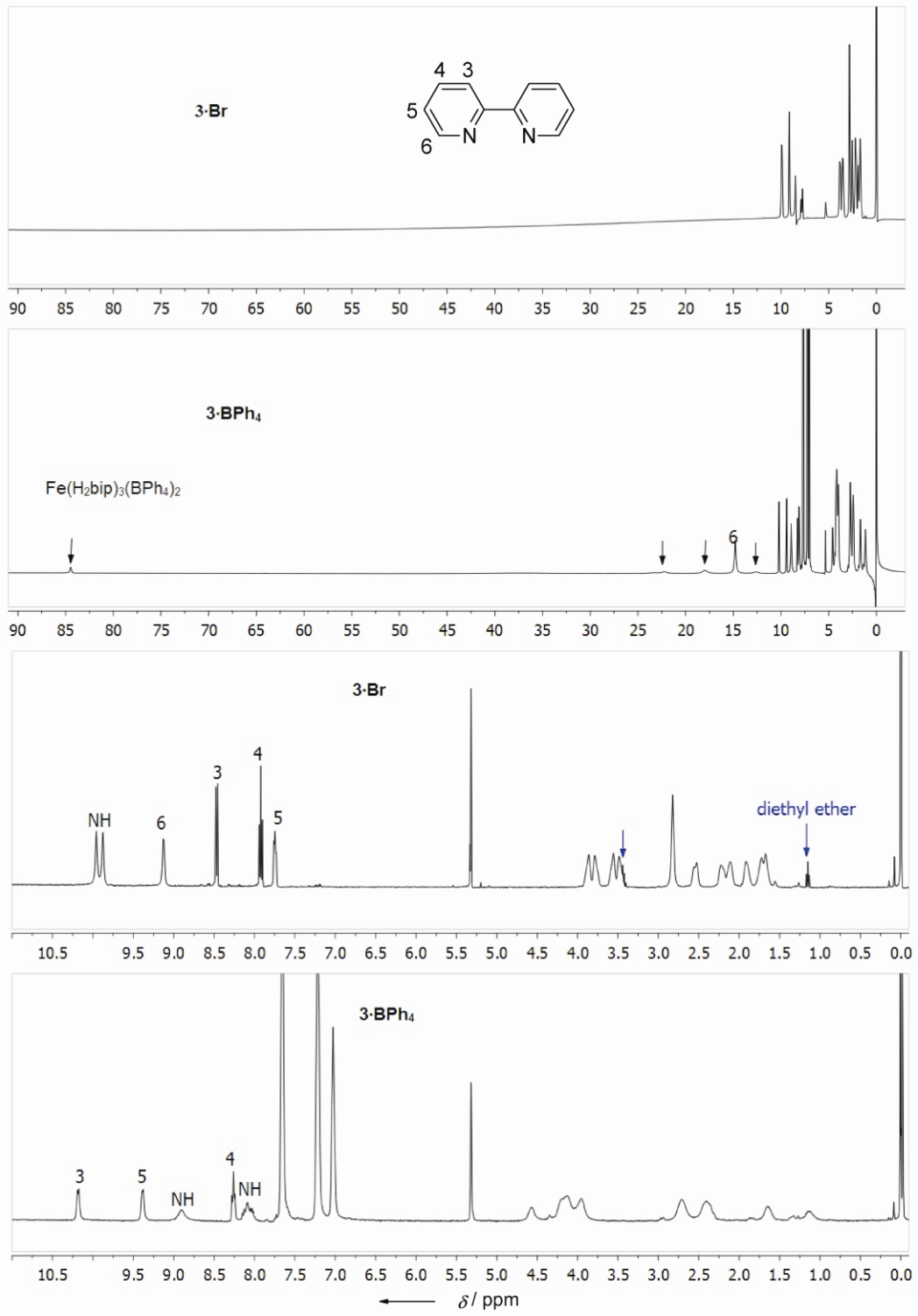

Figure S9. ^{1}H NMR spectra (expanded and normal windows) for salts of bpy-containing **3** at 296 K (400 MHz, CD_2Cl_2).

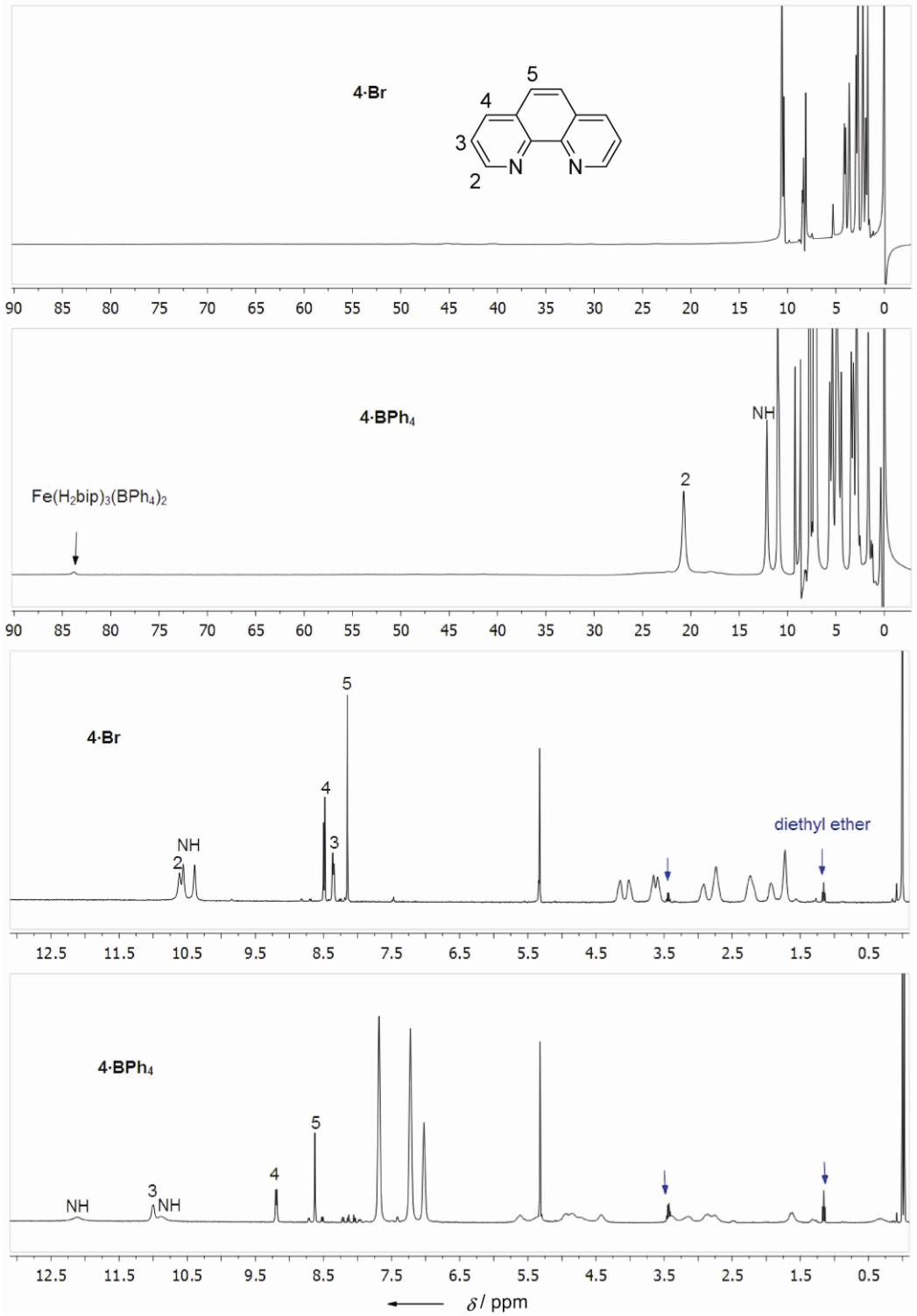

Figure S10. ^{1}H NMR spectra (expanded and normal windows) for salts of phen-containing **4** at 296 K (400 MHz, CD_2Cl_2).

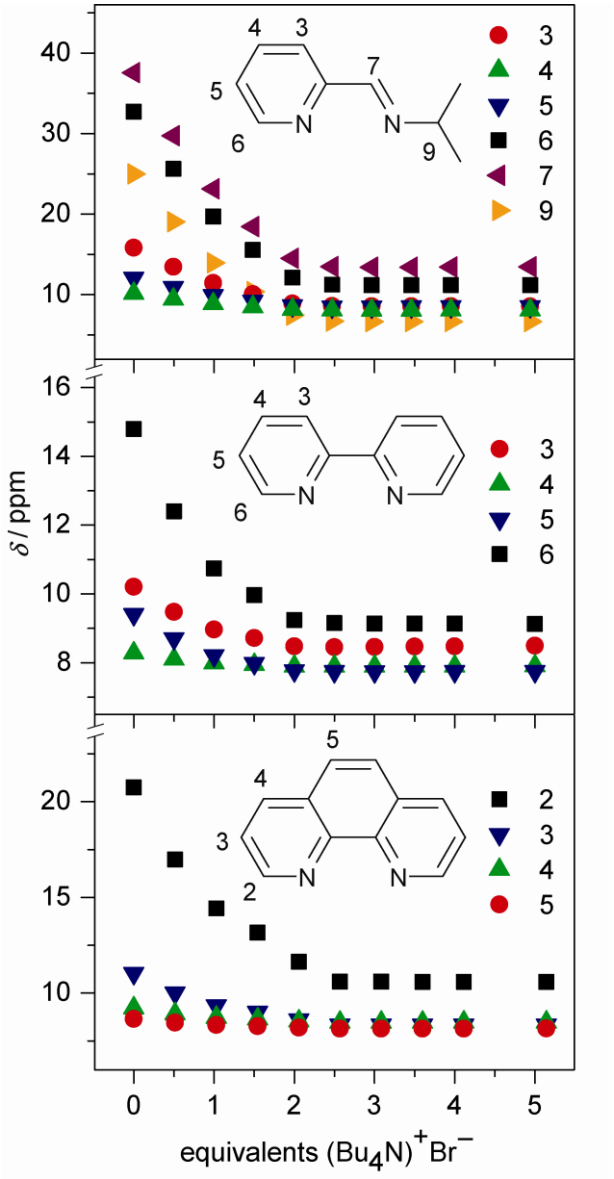

Figure S11. Change in chemical shifts of ancillary ligand (NN) protons at 296 K upon the addition of Bu_4NBr to (a) **2·BPh$_4$**, (b) **3·BPh$_4$** and (c) **4·BPh$_4$** in CD_2Cl_2.

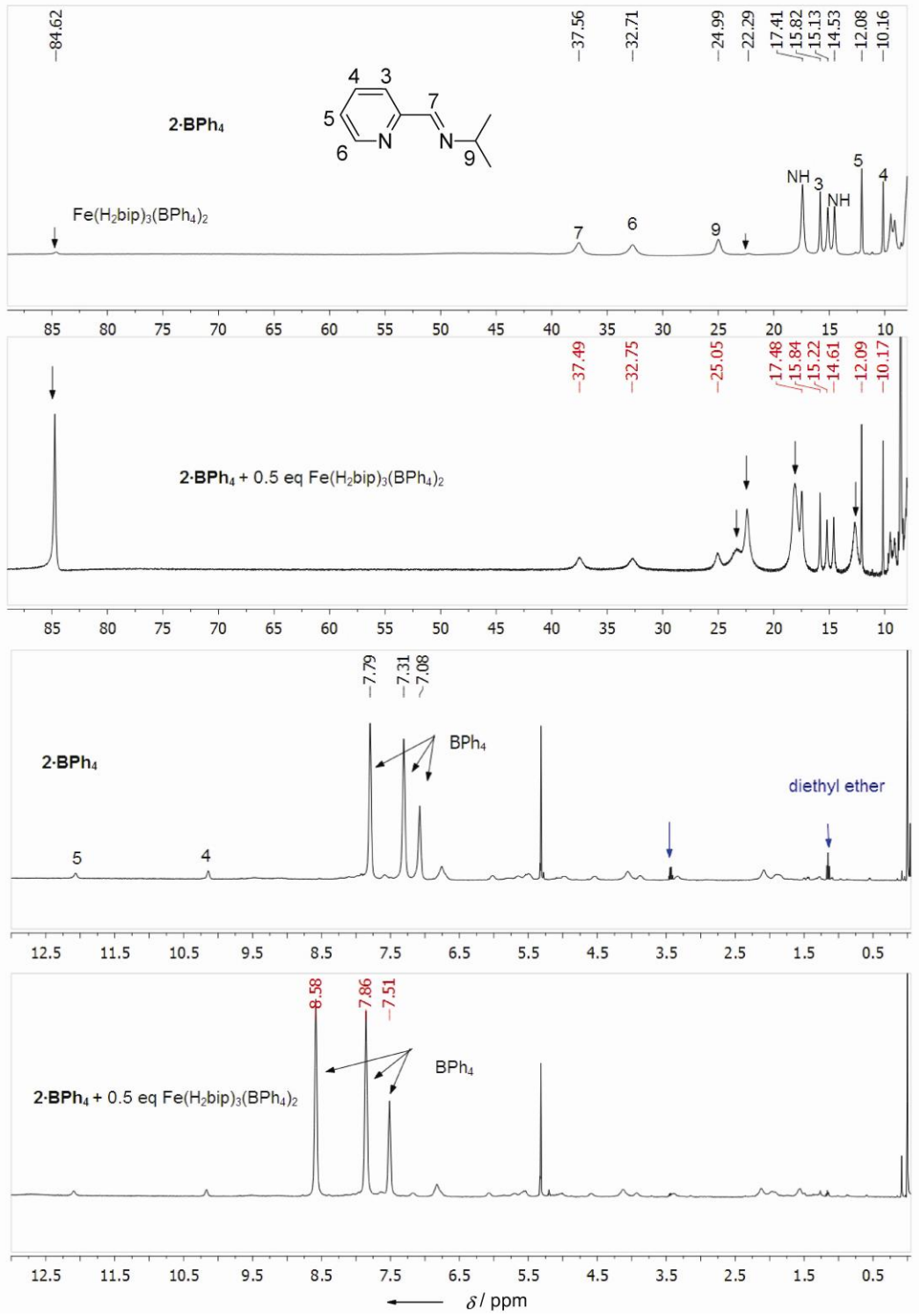

Figure S12. ^{1}H NMR spectra of **2·BPh$_4$** without and with 0.5 eq $Fe(H_2bip)_3(BPh_4)_2$ at 296 K (400 MHz, CD_2Cl_2).

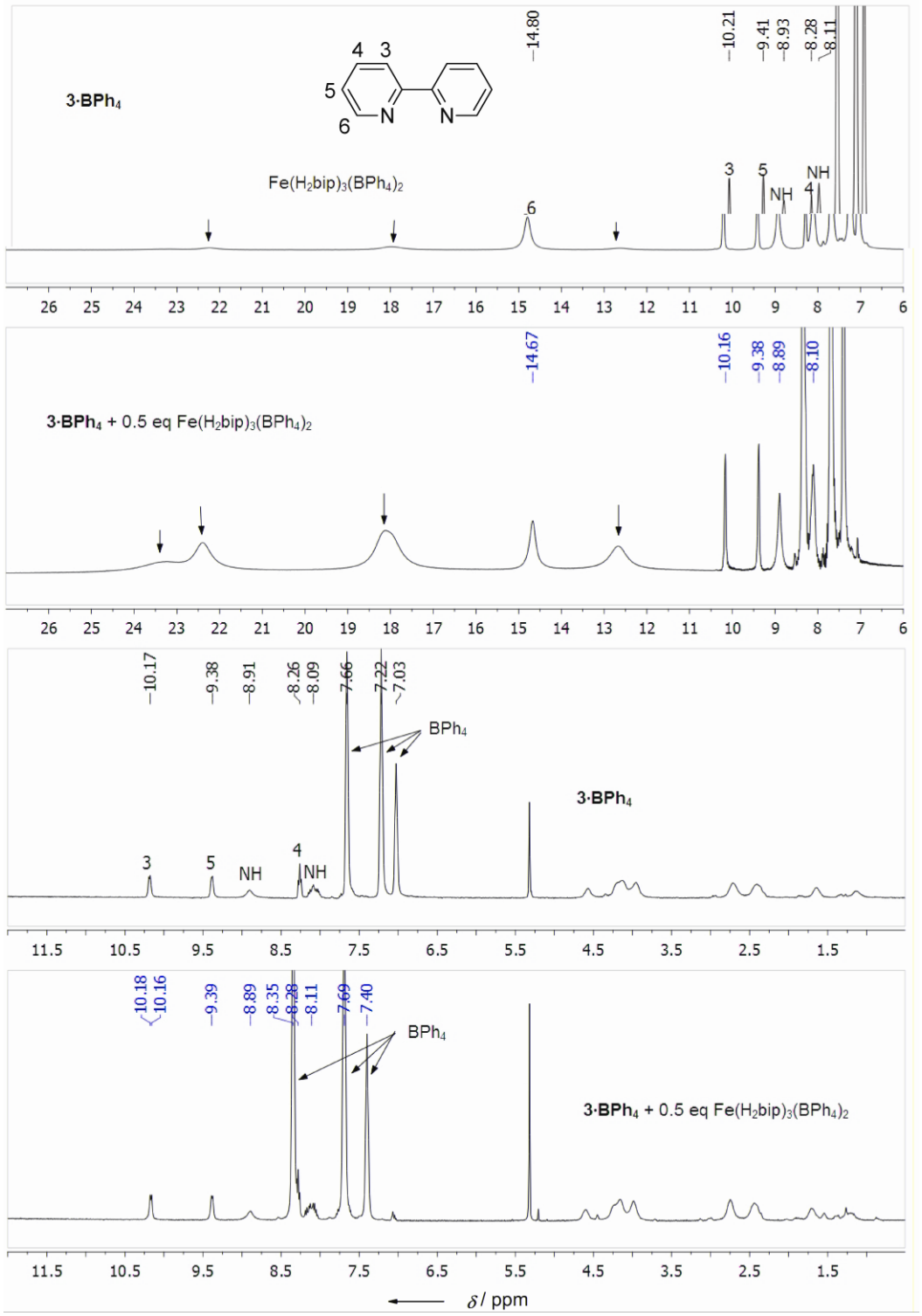

Figure S13. ^{1}H NMR spectra of **3·BPh$_4$** without and with 0.5 eq $Fe(H_2bip)_3(BPh_4)_2$ at 296 K (400 MHz, CD_2Cl_2).

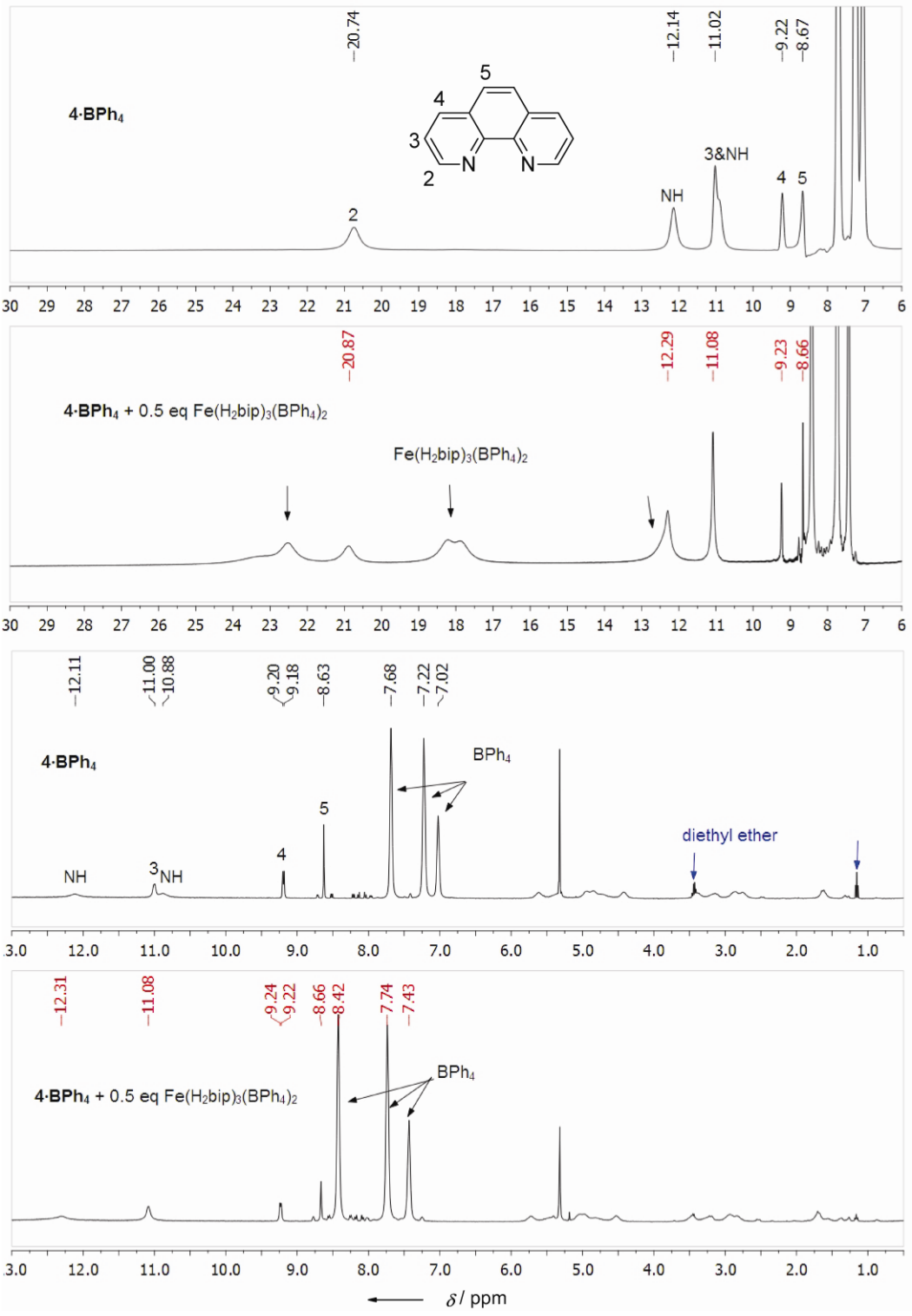

Figure S14. ^{1}H NMR spectra of **4·BPh$_4$** without and with 0.5 eq $Fe(H_2bip)_3(BPh_4)_2$ at 296 K (400 MHz, CD_2Cl_2).

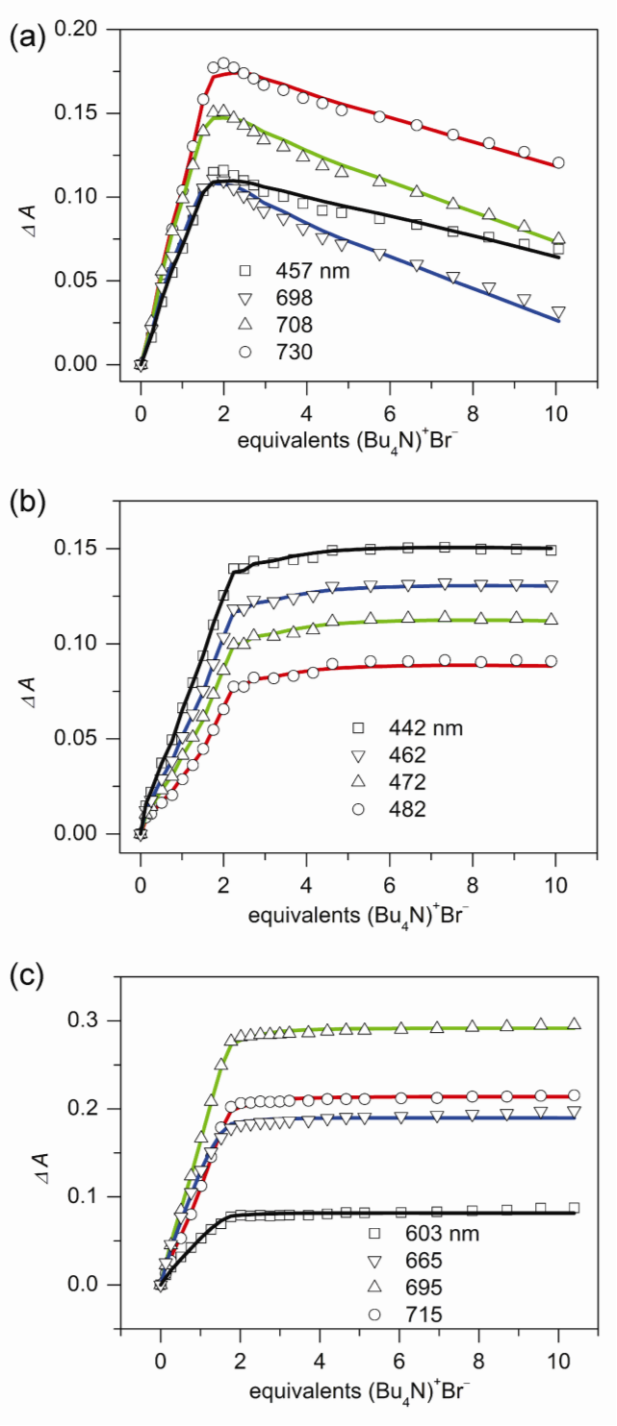

Figure S15. Binding isotherms with fitted curves (4K model) when CH_2Cl_2 solutions of (a) **2·BPh$_4$**, (b) **3·BPh$_4$** and (c) **4·BPh$_4$** are titrated with Bu_4NBr.

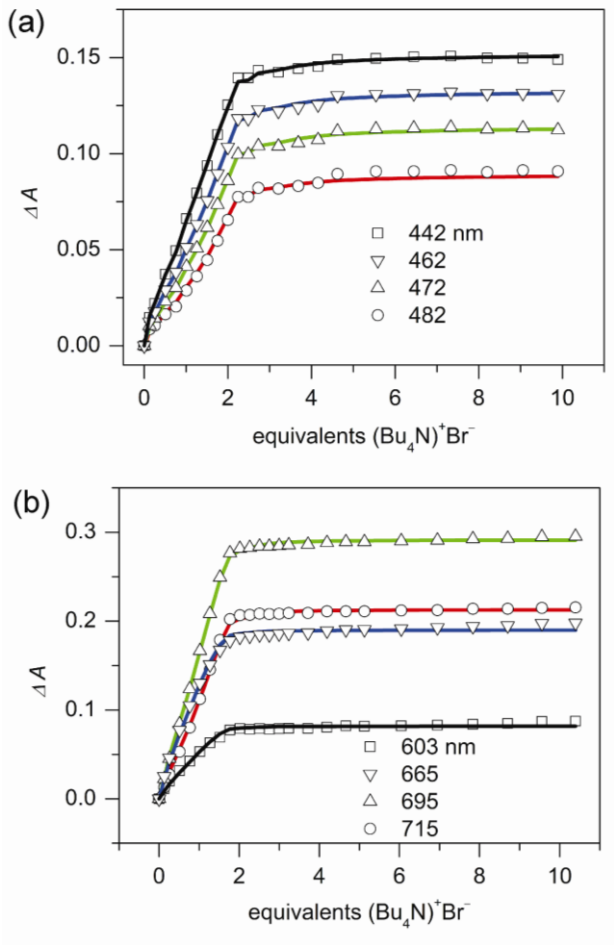

Figure S16. Binding isotherms with fitted curves (2K model) when CH_2Cl_2 solutions of (a) **3·BPh$_4$** and (b) **4·BPh$_4$** are titrated with Bu_4NBr.

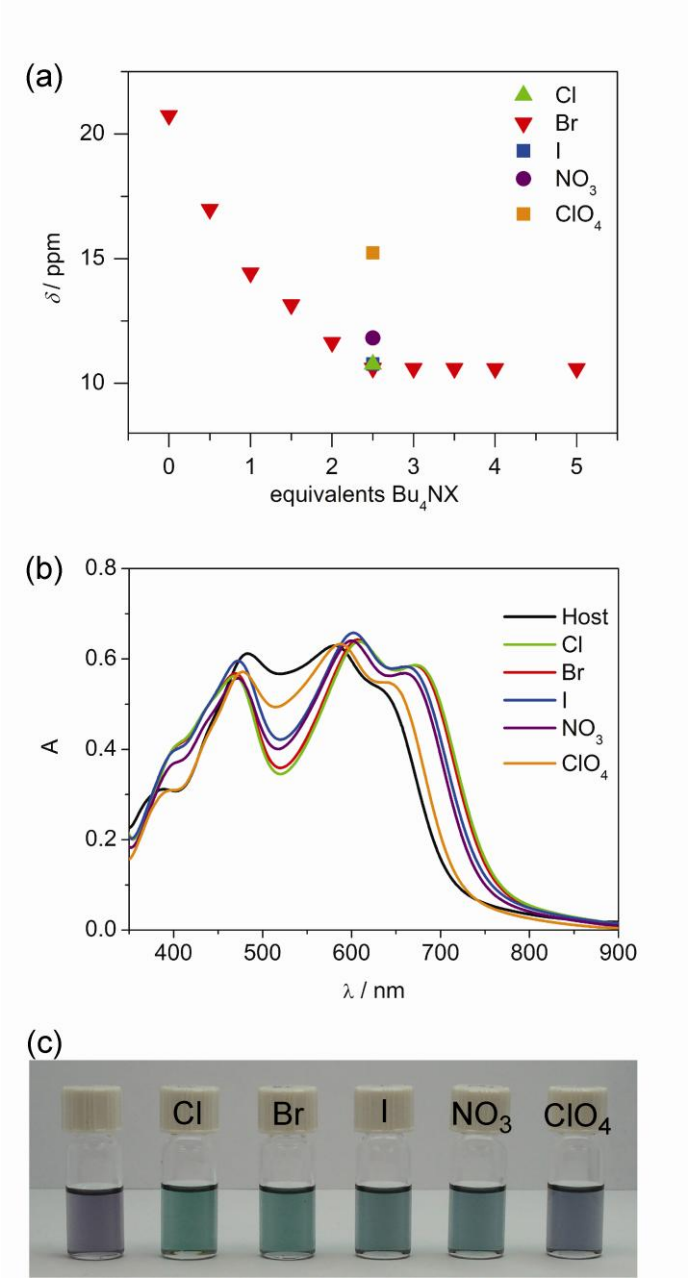

Figure S17. Changes in (a) chemical shifts of α proton on the phen ligand, (b) electronic absorptions and (c) colour (1.1×10^{-4} M) for **4·BPh$_4$** upon the addition of 2.5 equivalents of Bu_4NX (X = Cl, Br, I, NO_3, ClO_4). Changes in chemical shifts upon different equivalents of Bu_4NBr are shown in (a) for comparison.